ELSEVIER

Surface Science 437 (1999) 362–376

surface science

www.elsevier.nl/locate/susc

Methyl chemisorption on Ni(111) and C—H—M multicentre bonding: a density functional theory study

A. Michaelides, P. Hu *

School of Chemistry, The Queen's University of Belfast, Belfast BT9 5AG, UK

Received 18 March 1999; accepted for publication 28 May 1999

Abstract

Density functional theory has been used to study the adsorption of CH_3 on Ni(111). CH_3 is found to adsorb strongly at all four high symmetry sites of the Ni(111) surface. Calculated adsorption energies of CH_3 on the different sites are in the following order: hcp ≈ fcc > bridge > top. The bonding and structures of CH_3 on the different sites are analysed in detail. An important factor, namely three-centre bonding between carbon, hydrogen and nickel which contributes to the 'soft' C—H vibrational frequency of CH_3 on Ni(111), and may determine the preferred chemisorption site, is stressed. © 1999 Elsevier Science B.V. All rights reserved.

Keywords: Chemisorption; Density functional calculations; Magnetic surfaces; Nickel

1. Introduction

The chemisorption and reaction of hydrocarbon fragments on catalytically active transition metal surfaces have been extensively studied due to the commercial importance of hydrocarbon formation reactions. Methyl groups have long been believed to be important intermediates in many of these catalytic reactions not least Fischer–Tropsch [1–5], methane partial oxidation [6–11] and fuel reforming [12–14]. Taking the Fischer–Tropsch Synthesis as an example, issues such as bonding, migration and coupling of the intermediate hydrocarbon fragments are essential in understanding this process. There is no doubt that an understanding of the bonding is a starting point. In the present study, we concentrate on bonding between the adsorbate and substrate, and CH_3 chemisorption on Ni(111) is used as a model system.

It was not until 1986 that Kaminskey et al. [15] detected the formation of methyl groups in the methanation of CO and H_2 on the Ni(111) surface. The following year, Ceyer et al. [16] spectroscopically identified methyl groups on a single crystal surface under UHV conditions. They concluded that the reason that methyl groups had not been observed previously was that they were not stable to dissociations or recombinations above 150 K, well below the temperatures at which most catalytic reactions are performed. As a consequence of this instability, direct experimental data about the chemistry of these adsorbed species are difficult to obtain. The objective of much of the experimental work has been to map out the pathways and kinetics of reactions involving methyl groups on the surface. Ceyer et al. [17–20] obtained adsorbed methyl groups by the dissociative chemisorption of methane under UHV conditions and used iso-

* Corresponding author. Fax: +44-1232-382117.
E-mail address: p.hu@qub.ac.uk (P. Hu)

0039-6028/99/$ – see front matter © 1999 Elsevier Science B.V. All rights reserved.
PII: S0039-6028(99)00700-1

topic studies and high-resolution electron-energy-loss spectroscopy to ascertain further information. For CH_3 on Ni(111), they concluded that it is adsorbed at the threefold hollow sites with C_{3v} symmetry. Above 150 K, CH_3 dissociates, and at >250 K, C—C coupling occurs. Zaera and co-workers [21–25] as well as Bent and co-workers [26–29] have generated CH_3 groups on various transition metals from adsorbed methyl halides, and both groups have examined the balance between oxidative addition, reductive elimination and C—C coupling.

Direct experimental determinations of the relative stabilities of CH_x fragments have proved elusive. Information on the stabilities, therefore, has to be taken from theoretical calculations. Yang and Whitten [30,31] have carried out a substantial part of the theoretical work done on CH_x fragments on transition metal clusters. They performed ab-initio embedded cluster calculations to model CH_x fragments on Ni(111) and found that all CH_x fragments bind strongly at threefold and bridge sites. Adsorption energies, Ni—C bond lengths and C—H stretching frequencies were calculated, and an explanation of the methyl Ni bonding was included. Siegbahn et al. [32] and Schule et al. [33] also carried out bond-prepared cluster calculations to model CH_3 chemisorbed on Ni(100) and Ni(111). Calculated adsorption energies and optimised structures were given at all high symmetry sites. Van Santen and co-workers [34–38] carried out density functional calculations on methane activation and dehydrogenation in which the specific adsorption sites of CH_x fragments were discussed. Recently, Paul and Sautet [39] also using density functional methods, studied CH_x chemisorption on Pd(111). Extended Huckel methods have also been widely used to study such systems. Chemisorption of hydrocarbon fragments on Ni(111) has been studied by Gavin et al. [40] and methyl adsorption on Pt(111) by Minot [41]. A special mention should be made with regard to the work of Hoffmann and co-workers [42]. They studied the bonding and coupling of CH_3 on Co, Cr and Ti, providing some insight into the chemistry of these processes.

A particularly contentious issue with regard to hydrocarbon adsorbates on transition metal surfaces is the unusually 'soft' C—H stretching frequency often observed. Many explanations for its presence have been proffered. Some suggest that it results from an attractive hydrogen–metal interaction [43–46], whereas others believe the interaction to be repulsive [47]. Demuth et al. [43], amongst others, concluded that this phenomenon is directly related to one of the most basic and important processes in chemistry, namely C—H bond dissociation. Adsorbed methyl is one of the hydrocarbons that exhibits such a softened stretching frequency, and one of the objectives of this study is to shed some light on this issue.

We present here the first spin-polarised gradient corrected density functional theory calculations for methyl chemisorption on an extended nickel surface. The paper is organised as follows. Below, some of the details behind our total energy calculations are outlined. We report and discuss our results in Section 3. In Section 3.1, a brief comparison between spin-polarised and non-spin-polarised calculations is made. In Section 3.2, adsorption energies at the various sites are reported. Section 3.3 deals with the adsorbate structures obtained. A detailed analysis of the methyl-nickel bonding is provided, and special attention is paid to the C—H—M interaction in Sections 3.4 and 3.5, respectively. The conclusions are outlined in the final section.

2. Calculations

Ab-initio total energy calculations within the density functional theory (DFT) framework were carried out in this study. The total energy program, CASTEP [48], was used throughout to obtain optimised structures and energies. The basis set consists of plane waves. A Fermi smearing of 0.1 eV was utilised, and the corrected energy extrapolated to zero temperature by the method of Gillan and De Vita [49,50], which considerably reduces the k-point sampling. The Ceperly–Alder [51] exchange correlation energy was employed in local density approximation (LDA) calculations, whereas the generalised gradient approximation of Perdew and Wang [52,53] was utilised in gradient-corrected (GGA) calculations. Gradient-corrected,

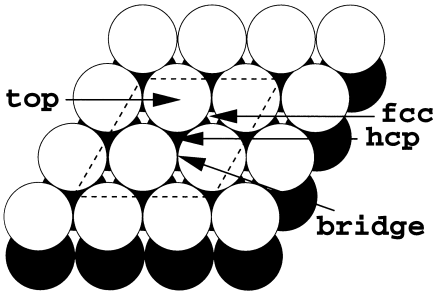

Fig. 1. Section of the Ni(111) surface. The arrows indicate the position of the four high-symmetry adsorption sites, and the dashed lines indicate the location of the surface unit cell. Only two layers of metal atoms are shown for clarity.

spin-polarised calculations were also performed, employing the implementation of White and Bird [54]. It has been found that gradient corrections are very important in first-principles, spin-polarised calculations of other systems [55–58]. All of the above (LDA, GGA and GGS) were used, self consistently, to achieve optimised geometrical structures. GGA and GGS alone were utilised to obtain energies. GGS calculations were also performed on the CH_3 radical in the gas phase.

Ab-initio non-local pseudopotentials [59] of C, H, and Ni in fully separable Kleinman–Blylander form [60] up to a 550 eV cut-off were used. The supercell approach was employed to model periodic geometries. The Ni(111) surface was represented by a three-layer Ni slab. Ni atoms were fixed at bulk truncated positions with a large vacuum region between slabs. A $p(2\times2)$ unit cell was used (Fig. 1), and CH_3 was placed on one of the two surfaces, corresponding to a coverage of 0.25 of a monolayer. A Monkhorst–Pack mesh [61] with $2\times2\times1$ k-grid sampling, in the surface Brillouin zone was used.

We checked that the properties of the isolated systems were accurately reproduced. Table 1 compares the calculated and experimental [62] bond lengths and bond angles of CH_3 and CH_4. Table 2 compares the calculated and experimental lattice constants of Ni. It is clear from Tables 1 and 2 that there is good agreement between calculated and experimental values. Tests concerning the accuracy of the chemisorption model were also performed. First of all, the chemisorption energy of CH_3 adsorbed upon a four-layer slab was calculated. The difference in chemisorption energy between the four-layer and three-layer slab was found to be $\sim$0.01 eV. Second, the adsorbate was placed on both sides of the four-layer slab. In this case, the absolute chemisorption energy differed from the three-layer calculation by $\sim$0.06 eV. Third, the convergence of the chosen cut-off energy was tested. This was done by calculating the chemisorption energy of CH_3 with a 620 eV cut-off energy. A $\sim$0.01 eV between the 620 and 550 eV cut-off energies was found. Calculations were also performed in which the top layer of Ni atoms of the three-layer slab were allowed to relax. In this case, the chemisorption energy difference between

Table 1
Comparison between calculated and experimental structural parameters of free CH_3 and CH_4[a]

	C—H (Å)			C—H angle (degrees)	
	Experimental	GGA	GGS	Experimental	GGA/GGS
CH_3	1.08	1.09	1.08	120.0	120.0
CH_4	1.09	1.09	–	109.5	109.5

[a] GGA is the generalised gradient approximation. GGS is the spin-polarised generalised gradient approximation.

Table 2
Comparison between calculated and experimental bulk lattice constants of Ni

	Experimental	LDA	LSDA	GGA	GGS
Lattice constant (Å)	3.5238	3.5323	3.5478	3.5685	3.5122

the relaxed and unrelaxed systems was calculated to be ~ 0.05 eV. Structure optimisations were performed in all of the above tests, and the structural differences were found to be very small, typically ~ 0.01 Å. Therefore, we feel confident that the model used offers a high level of precision for this system and is the best compromise between accuracy and computational load.

3. Results and discussion

3.1. Comparison between spin-polarised and non-spin-polarised calculations

It is well known that nickel is ferromagnetic. It has been found that adsorbates generally reduce the magnetic ordering of nickel, particularly in the bonding region between adsorbate and substrate [63,64]. There have been several reports about the geometrical structure of CH_3/Ni(111). Interestingly, they all resulted from theoretical calculations, and experimental structure determination is still lacking. Although all the structures reported are similar, differences are apparent. In order to find out what effect the magnetic properties of the surface have on the global properties (adsorption energies, geometrical structure) of the adsorption system, we carried out both GGA and GGS structure optimisations. The chemisorption energies, E_{ads}, were also calculated:

$$E_{ads} = E_{CH_3/Ni} - E_{Ni} - E_{CH_3},$$

where $E_{CH_3/Ni}$, E_{Ni}, E_{CH_3} are the total energies of Ni(111)—p(2×2)—CH_3, Ni(111) and CH_3, respectively. Table 3 compares the E_{ads} calculated from both GGA and GGS. It is clear that the GGA calculations tend to overestimate the E_{ads} by approximately 0.25 eV. This is because in the GGS calculations, it was found that, at all sites, approximately one surface magnetic moment was lost upon adsorption. More significantly, the overbinding predicted by the GGA manifests itself in the optimised structural parameters. The methyl fragment rests closer to the surface, and consequently, the C—Ni bond length, at the hcp site for example, is 2.19 Å from GGA compared to 2.28 Å from GGS. This shorter C—Ni bond length produces some reorganisation within the CH_3 adsorbate. This can be seen in Table 4, which compares the main structural parameters obtained from both methods, as well as from the LDA. A noticeable feature of Table 4 is the longer C—H bond lengths predicted by the LDA and GGA. This is a consequence of the stronger C—Ni bonding, and as we shall see in Section 3.5, the C—H bond length is related to the H—Ni distance. This comparison helps to explain the differences in structures reported from CI (configuration interaction) and DFT methods. By comparing Tables 4 and 5, it is clear that the LDA calculations of Kratzer et al. [65] are close to ours, whereas the CI calculations of Yang et al. [30,31] and Schule et al. [33], which include spin, agree favourably with our GGS calculation. These results also offer suggestive evidence for the Magnetocatalytic effect [66,67]. As the magnetic nature of the substrate diminishes (going from GGS to GGA), the reactivity of the substrate appears to change; the adsorbates bind to the substrate in a distinguished manner, and the chemisorption energies on the high symmetry sites are different. Such changes in the global properties of the adsorption system must affect the catalytic activity of the substrate. To conclude this subsection, it is clear that spin-polarised calculations are needed, at least at low coverages, in the calculation of both correct adsorption energies and structures for CH_3 on Ni(111). Because of this, all analyses and discussions will be based upon results obtained from GGS calculations.

Table 3
GGS and GGA adsorption energies on the four high symmetry sites of Ni(111). The geometries of hcp60 and fcc60 are shown in Fig. 2b[a]

	GGS (eV)	GGA (eV)	GGA[b] (eV)
hcp	1.48	1.74	1.63
fcc	1.46	1.72	1.65
bridge	1.37	1.64	1.63
top	1.22	1.51	1.52
hcp60	1.22	–	1.45
fcc60	1.26	–	1.42

[a] All energies are in electron-volts.
[b] S.C.F. GGA energies applied to LDA structures.

Table 4
Structural parameters obtained from GGS, GGA and LDA geometry optimisations for CH_3 adsorbed at the four high-symmetry sites of Ni(111)[a]

		C—H (Å)	C—Ni (Å)	$d_\perp$ (Å)	H—M (Å)	α1 (degrees)	α2 (degrees)
GGS							
hcp		1.10	2.28	1.76	2.21	107.02	111.81
fcc		1.10	2.28	1.76	2.21	106.95	111.89
bridge	$H_{b/c}$	1.10	2.20	1.80	2.21	108.86	108.23
	H_c	1.09			2.50	105.54	116.56
top		1.09	2.01	2.01	2.59	109.24	109.71
GGA							
hcp		1.11	2.19	1.65	2.10	106.99	111.86
fcc							
bridge	$H_{b/c}$	1.10	2.15		2.20	108.17	108.75
	H_c	1.10			2.52	105.43	116.75
top							
LDA							
hcp		1.13	2.05	1.46	1.94	106.53	112.27
fcc		1.13	2.07	1.48	1.95	106.37	112.42
bridge	$H_{b/c}$	1.13	2.05	1.61	2.05	108.45	108.81
	H_a	1.10			2.34	104.09	117.36
top		1.10	1.98	1.98	2.89	109.00	109.91

[a] $d_\perp$ is the carbon surface distance. α1 and α2 are the H—C—H and surface—C—H angles, respectively. The hydrogens at the bridge site are inequivalent and are therefore labelled (see Fig. 3.).

3.2. CH_3 adsorption

The Ni(111) surface exhibits four high-symmetry adsorption sites: top; bridge; and two threefold hollow sites, shown in Fig. 1. The threefold hollow sites differ only in their relationship with the second layer. The hcp threefold hollow site has a Ni atom directly below it, whereas the fcc threefold hollow site has a Ni atom only in the third layer. CH_3 is found to bind strongly to all four sites of the Ni(111) surface. Calculated chemisorption energies are 1.48, 1.46, 1.37 and 1.24 eV for adsorption at the hcp, fcc, bridge and top sites, respectively. Clearly, the threefold hollow adsorption sites are the most stable with the difference between them being only 0.02 eV. These results indicate that the potential energy surface for diffusion is quite flat.

The energy of adsorption for CH_3 on Ni(111) has not been experimentally measured. Such a value is difficult to determine and requires very accurate calorimetric measurement. A theoretical approach is therefore useful. Much debate surrounds the preferred adsorption site for methyl on Ni(111). In two of the most recent theoretical studies on this system, both Yang et al. [30,31] and Schule et al. [33] find the threefold sites to be

Table 5
Main structural parameters reported from other theoretical studies for CH_3 adsorption on Ni(111)

	C—H (Å)	C—Ni (Å)	$d_\perp$ (Å)	α2 (degrees)
Yang et al. [30,31]				
hcp		2.35	1.86	~112
fcc		2.34	1.94	
bridge		2.33	1.84	
top		2.03	2.03	
Schule et al. [33]				
hollow	1.10		1.91–1.96	112
top	1.09		1.87–2.08	108–110
Kratzer et al. [65]				
hollow	1.18		1.56	
top			1.94	

the most stable. Yang et al. obtained values of 1.68–1.47 eV for hollow and top sites, respectively, which are approximately 0.2 eV lower than our results. A similar order of stabilities was also reported (hcp = fcc > bridge > top). Schule et al. reported energy ranges of 1.95–2.2 eV for hollow site adsorption and 1.87–2.08 eV for on-top adsorption. These are higher than our results, although a similar difference between hollow and top sites was reported. Recently, Van Santen and co-workers [34–38], using density functional theory cluster calculations, found that adsorption on the top site of a Ni(111) cluster was most favourable. Their reported trend for E_{ads} is top > bridge > hollow. As we have shown, we found the opposite to be true. Extended Huckel calculations also favour adsorption on the top site over the hollow sites [41,42]. However, most ab-initio calculations seem to agree that the hollow sites are the most stable, and the only available experimental data for CH_3 on Ni(111) favour hollow site adsorption [20].

3.3. Structure of adsorbed CH_3

3.3.1. hcp and fcc threefold hollow sites

We begin by examining the most stable adsorption sites: the threefold hollow sites. In fact, the optimised structures obtained at these sites are practically identical. CH_3 is adsorbed with C_{3v} symmetry, and carbon sits in the hollow site with the hydrogens in a plane parallel to the surface. The CH_3 pyramid is somewhat squeezed with a H—C—H angle of $\sim 107^\circ$ ($\alpha 1$) compared to the tetrahedral value of 109.5° for CH_4. The surface—C—H angle ($\alpha 2$) is $\sim 112^\circ$. Two arrangements for the hydrogens have been considered. In the first, each hydrogen points towards its nearest Ni neighbour, as shown in Fig. 2a, and in the second, the hydrogens point towards their closest bridge sites, shown in Fig. 2b. Throughout this paper, structure (a) will usually be referred to as fcc/hcp, and structure (b) as fcc60/hcp60. Yang and Whitten [30,31] found that structure (a) is 0.18 eV more stable than structure (b). Kratzer et al. [65] found the difference, in the GGA, to be 0.17 eV. We found this difference to be 0.20 and 0.26 eV at the fcc and hcp sites, respectively. The energy differences between fcc/hcp and fcc60/hcp60 can be viewed in terms of a rotational barrier with the lowest point in energy occurring where the hydrogens point towards their nearest Ni neighbours. Yang and Whitten also examined rotational barriers at the bridge and top sites and found them to be substantially smaller. It is clear that it is energetically favourable for the hydrogens of the methyl to be alligned with the underlying surface Ni atoms. Favourable H—metal (H—M) alignments have been reported for other adsorbates; CH_2 [40], CH_3O [68], H_2O [69,70] and NH_3 [71]. The H—M distances in these cases are typically around 2 Å, well inside the sum of their Van der Waals radii (2.83 Å for H and Ni). Therefore, it is reasonable to assume that some sort of H—M interaction must be present. However, the nature of this H—M interaction is still unclear. In order to find out more about this interaction, structure optimisations of both (a) and (b) were carried out. We found that the C—H bond lengths in CH_3/Ni(111), 1.10 Å for the fcc and hcp sites, are longer than that of gaseous CH_3, which is 1.08 Å from both calculation and experimental work [62]. This can be attributed to C—H—metal (C—H—M) multicentre bonding (see Section 3.5). The C—H bond length in structure (a), 1.10 Å, was found to be longer than in (b), 1.09 Å for both the fcc and hcp sites. This indicates that the interaction between C, H and

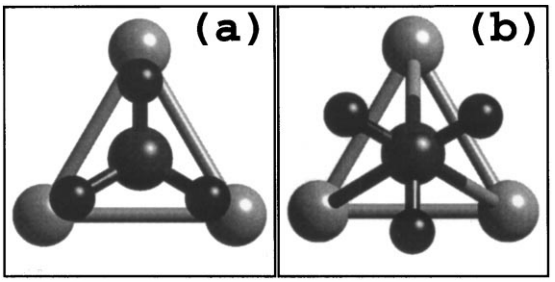

Fig. 2. Two possible orientations of CH_3 adsorbed at a threefold hollow site of Ni(111). (a) is the lower energy orientation, and (b) is 0.20 and 0.26 eV higher in energy at the fcc and hcp sites, respectively. Both structures are viewed from above the plane of the surface. The nickles are the largest spheres; only three of these are shown. The hydrogens are the smallest spheres and are in a plane parallel to the surface.

metal atoms in structure (a) is stronger than in (b). The C—Ni bond lengths also differ at fcc/hcp and fcc60/hcp60, being 2.28 and 2.32 Å, respectively. Tables 4 and 5 compare the main structural parameters calculated with those of other recent theoretical studies.

3.3.2. bridge site

A noticeable feature of CH_3 adsorption at the bridge site is that the hydrogens no longer lie in a plane parallel to the surface. The plane of the hydrogen atoms is tilted by 4° from the horizontal, as shown in Fig. 3a. This results in two different values for α2; 108° for the two hydrogens (H_b and H_c) closest to the bridging Ni atoms and 117° for the third H (H_a), which is directed away from the bridge. Two different values for α1 were also obtained: 106° between H_b and H_c; 109° between H_a and H_b/H_c, shown in Fig. 3b. The three C—H bonds also differ in length. The two C—H bonds closest to the bridging Ni atoms are 1.10 Å, whereas the third H atom has a bond length of 1.09 Å. The H—Ni distance for the two hydrogens closest to the bridging Ni atoms is 2.21 Å. The third hydrogen is 2.50 Å away from its nearest Ni neighbour. It is clear, therefore, that the hydrogens are no longer equivalent. As we shall see, the peculiarities of the bridge site can be explained effectively within the three-centre bonding model (see Section 3.5). As expected, the C—Ni distance of 2.20 Å is shorter than that at the hollow sites.

3.3.3. top site

As at the hollow sites, the hydrogens are equivalent and lie in a horizontal plane. Moreover, the adsorbed methyl most closely approximates the tetrahedral structure of methane on this site. Both α1 and α2 are ~109° (Table 4). The C—H bond length of 1.09 Å is shorter than that at other sites, although it is still longer than the gas-phase value of 1.08 Å. The H—Ni distance, 2.59 Å, is close to the sum of their Van der Waals radii. It is no surprise that at such a distance, any Ni—H interaction will be small. The shortest C—Ni distance of 2.01 Å is found at this site.

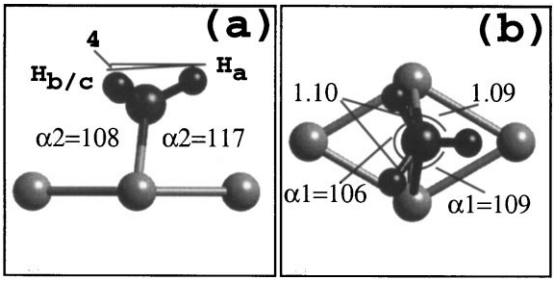

Fig. 3. Optimised structure of CH_3 adsorbed at the bridge site. (a) Side view. (b) View from above. Bond distances are in angstroms, and angles are in degrees.

3.4. Bonding

When considering the bonding of a CH_3 fragment to a metal surface, it is beneficial to first consider the orbitals of the methyl radical itself. Two-dimensional contour plots of electron densities are displayed in Fig. 4 for the four occupied orbitals of CH_3 in the gas phase. CH_3 has C_{3v} symmetry, and the orbitals are labelled accordingly.The energy level is low in the 2a1 orbital, higher in the 1e degenerate pair and higher still in the singly occupied 3a1 orbital (Fig. 7). The antibonding orbitals, $4a1^*$ and $2e^*$ are unocuppied. As adsorption at the hcp and fcc sites is lowest in energy, the bonding of CH_3 to these two sites will be examined thoroughly.

3.4.1. hcp and fcc threefold hollow sites

Yang and Whitten [30,31] suggested that the 3a1 and 1e orbitals are the main orbitals involved in bonding with the surface. They found, for all adsorption sites, that the 3a1 orbital forms a strong **σ** bond with the 4s orbitals of Ni and that the 1e orbitals interact with Ni 3d. The main 3a1–4s mixing occurs at 4.9 eV below the Fermi level, and the nearly degenerate 1e–3d levels are ~11 eV below the Fermi level [30,31]. Hoffmann and co-workers [42] analysed their extended Huckel calculations using decompositions of densities of states and crystal orbital overlap populations and suggested that the 3a1 orbital is important in adsorbate–substrate bonding for CH_3 adsorbed on Co, Cr, and Ti.

It was generally believed that the 2a1 orbital, the lowest occupied valence orbital in CH_3, is too low in energy to have an effective interaction with the metal substrate. However, we found that the

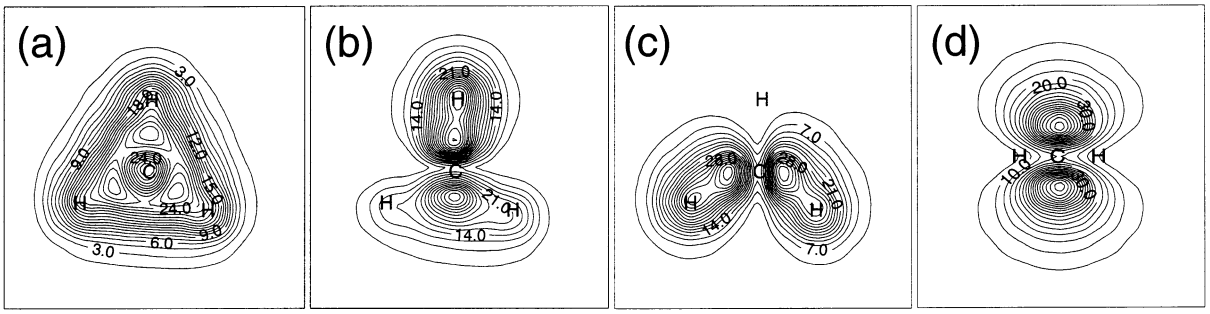

Fig. 4. Two-dimensional electron density contour plots (a–d) for the four occupied orbitals of gas phase CH_3. (a) is the lowest energy 2a1 orbital. (b) and (c) are the 1e degenerate pair. (d) represents the HOMO; 3a1. (a)–(c) are viewed from above the plane of the molecule, and (d) is viewed from the side. The density is plotted in units of 7.65×10^{-6} electrons bohr^{-3}.

energy of the 2a1 orbital drops by more than 1 eV upon adsorption to 13.2 eV below the Fermi level. A careful examination of the quantum states shows a noticeable mixing between the 2a1 and Ni 3d states. This is highlighted in Fig. 5, in which the difference between the 2a1 orbital of CH_3 in the same structure as CH_3 on the hcp site of Ni(111) and the first orbital (2a1 derived) of CH_3/Ni(111) is shown. It can be seen that although not strong there is (1) an electron delocalisation towards the metal; and (2) 2a1–d mixing occurs.

The 1e molecular orbitals mix with Ni 3d orbitals. In fact, strong three-centre bonds between C, H and Ni are created. This is, we believe, the origin of the much debated H—M interaction. A separate section, Section 3.5, is devoted to their discussion.

A dramatic change in the 3a1 orbital occurs upon adsorption. There is strong mixing between the 3a1 orbital and metal 3d states. A quantum state of this type is shown in Fig. 6. This mixing results in a substantial decrease in the energy of the 3a1 orbital by up to 5 eV, and the main 3a1–d mixing occurs $\approx$4.6 eV below the Fermi level. States of this type are also observed at higher energies. From Fig. 6, it is clear that a strong **σ**-type bond has been created with the surface. It also shows that this 3a1 derived state is now a bonding orbital with respect to CH_3 because of charge accumulation between C and H, whereas it was non-bonding prior to adsorption. This is because the three hydrogens are no longer in a

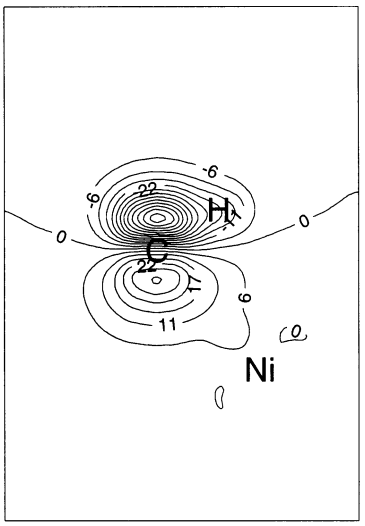

Fig. 5. Electron density difference plot between the 2a1 orbital of CH_3/Ni(111) and the 2a1 orbital of gas phase CH_3 in the same structure as that at the hcp site. The plane is through C, Ni and H: perpendicular to the surface. Negative (positive) values represent a decrease (increase) in density upon adsorption. The density is plotted in units of 7.65×10^{-6} electrons bohr^{-3}.

plane with the carbon. Fig. 7 is a plot of local density of states within a sphere cut around carbon. The position of the CH_3 molecular orbitals is also indicated, and it is clear how these orbitals have moved upon adsorption. The lowest energy peak corresponds to the 2a1 derived orbital, next in energy are the 1e derived states, and the broad peak between -10.0 and -7.0 eV corresponds to 3a1 derived states.

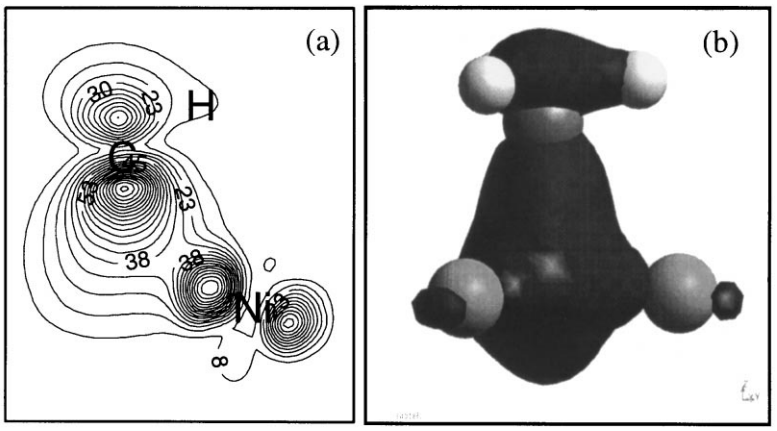

Fig. 6. Two-dimensional electron density contour plot (a) and a three-dimensional isosurface (b) representing 3a1–d mixing. The 2D slice is perpendicular to the surface, cutting through the C—Ni bond. The density is plotted in units of 7.65×10^{-6} electrons bohr^{-3}.

3.4.2. bridge site

On the whole, bonding at the bridge site is weakened compared to the two threefold sites. The 3a1–d mixing, although weakened somewhat, remains strong. The main reason for decreased stability arises from a weakening of the 2a1–3d delocalisation and 1e–d mixing. The 2a1 derived quantum state is 0.1 eV higher in energy than at the hcp site. Carbon now only has two neighbours with which it can mix. The near degeneracy of 1e derived quantum states is lost because the three hydrogens are no longer equivalent. One of these states is pushed up in energy by 0.2 eV because multicentre bonding (see Section 3.5) is weakened due to a greater H—Ni distance.

3.4.3. top site

Bonding is less favourable on the top site than on other sites. 3a1–d mixing is weakened and occurs at higher energies. However, as at the bridge site, the main reason for decreased stability is a weakening of 2a1 and 1e mixing. The 2a1 derived orbital is 0.8 eV higher in energy than at the hcp site. The reason for the increase in energy of 2a1 and 3a1 derived states is that CH_3 only interacts with one Ni atom. The 2a1 derived state is mixed and polarised less than it is at the hcp site. The 1e derived states are also higher in energy, close to their gas-phase energy. This is because 1e–3d mixing is very weak at this site, due to a larger H—Ni separation.

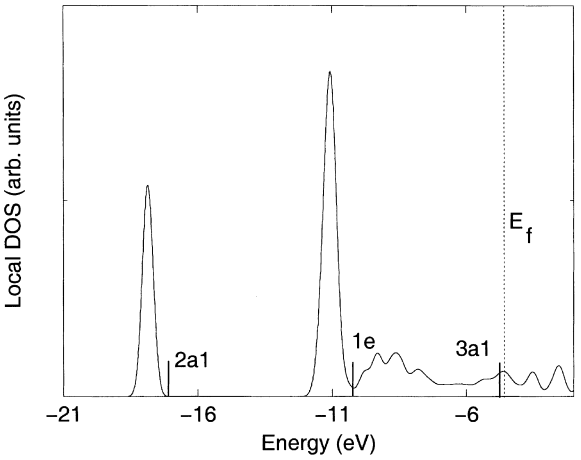

Fig. 7. Local density of states around C when CH_3 is adsorbed at the hcp site of Ni(111). The thicker straight lines indicate the position of the CH_3 molecular orbitals prior to adsorption.

3.4.4. General features for the four different sites

It has been suggested that charge transfer from the surface towards the adsorbate is an important aspect of the adsorbate–substrate bonding in this type of system. The rationale for this is based upon the desire to fill the singly occupied 3a1

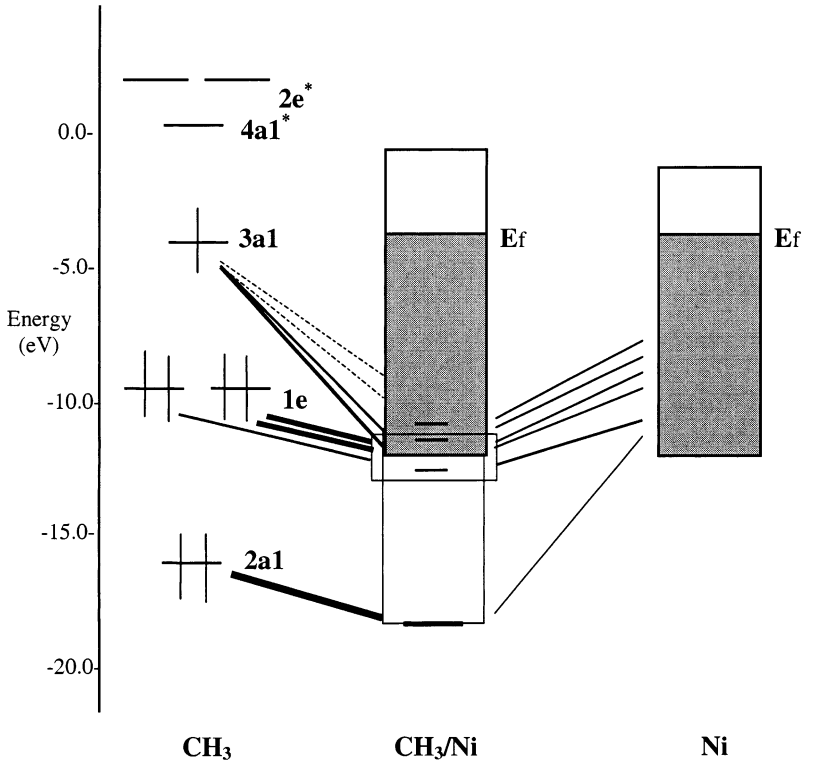

Fig. 8. Schematic molecular interaction diagram of the Ni(111)–p(2 × 2)–CH_3 adsorption system. The derivation of some states that are important in adsorbate–substrate bonding are indicated by diagonal lines. The thicker the diagonal line, the larger the contribution from a particular state.

orbital. Yang and Whitten [30,31] found that the net charge transferred to carbon at the hcp site is 0.54 electrons, 0.4 from the surface and 0.14 from the hydrogens. Hoffmann and co-workers [42] found that the 3a1 orbital changes its occupation from 1.0 in free methyl to 1.52 at the hollow sites. They also identified an ionic nature to the bonding between CH_3 and the substrate. Calculating the precise extent of electron charge transfer can be a contentious issue; nevertheless, we estimated it by cutting spheres around Ni, C and H before and after adsorption, calculating the total density within these spheres and noting what changes, if any, had occurred. At variance with previous studies, no significant charge transfer towards the methyl group was observed. The 3a1 derived orbital does become fully occupied, but the electrons in this orbital are shared between C and Ni. In fact, the electron density in the core region of C is found to decrease slightly, while that in the valence region increases. This is indicative of a general trend in both C and Ni, with the extent of charge transfer being very similar at all the high-symmetry adsorption sites. Prior to adsorption, the electrons are more contracted, resulting in a larger electronic density in the core region, and upon adsorption, density is transferred into the bonding region between adsorbate and substrate. This result indicates that the C—Ni interaction does not involve a large amount of intersite charge transfer between C and Ni but instead resembles covalent bonding. The interaction between CH_3 and Ni(111) is summarised in the schematic diagram shown in Fig. 8. The low-energy orbitals of the CH_3/Ni(111) system are presented as thick lines, indicating that they are in an energy band rather than at discrete levels due to their solid-state properties. Analogous interaction diagrams

have been proposed recently for CO on various transition metals [72–74].

3.5. C—H—M multicentre bonding

'Soft' C—H vibrational frequencies of hydrocarbons, e.g., methyl fragments, adsorbed on transition metal surfaces have often been observed. This 'soft' vibrational frequency is important because it may signify a weakening of the C—H bonds within the fragments, and an understanding should shed some light upon how these fragments dehydrogenate. For CH_3 on Ni(111), this 'soft' C—H stretching frequency occurs at 2680 cm^{-1} [20], which corresponds to a red shift of approximately 300 cm^{-1}, compared to the usual gas-phase C—H stretching frequency of $\approx$3000 cm^{-1}. The physical origin of this shift is in much debate. Demuth et al. [43], who first observed a shift of similar magnitude for cyclohexane adsorbed on Ni(111) and Pt(111) and ethylene on Pt(111), suggested that a hydrogen-bonding interaction was present between a H of the adsorbate and the surface. They proposed that this interaction modified the shape of the C—H vibrational potential and lowered the activation barrier to C—H bond breakage. Whether or not the physical reason for mode softening in larger saturated hydrocarbons is the same for mode softening in adsorbed methyl is not clear, but we believe that it is constructive to test this hydrogen-bonding model to see if it holds for this system.

The distinguishing feature of hydrogen bonding is the involvement of one specific hydrogen atom of a proton donor group (A) with a proton acceptor group (B) giving rise to an A—H—B moiety consisting of a stronger A—H bond and weaker B—H bond, termed a hydrogen bond. Hydrogen bonding is mainly seen in cases where the proton is donated by hydroxyl, carboxyl, amine and amide groups. However, the hydrogen from a C—H group can also take part in hydrogen bonding, but generally, such bonds are weaker and occur less commonly [75,76]. For hydrogen bonding to occur in this system, the Ni surface will have to act as the proton acceptor group (B). In other words, the Ni surface would have a slightly negative charge. However, as we have seen, the Ni surface transfers electron density into the bonding region and is in fact slightly positively charged after adsorption. Therefore, hydrogen bonding can be ruled out as the reason for the 'soft' C—H frequency, for this system at least.

Several other explanations have been offered for C—H mode softening in hydrocarbons adsorbed on transition metals [20,33,43–47]. We will concentrate on those proposed for methyl. Schule et al. [33] have argued that the 'soft' C—H frequency occurs when CH_3 is adsorbed at hollow sites, and is a consequence of charge transfer from metal into C—H antibonding orbitals ($2e^*$). This view was shared by Bent and co-workers [29]. By altering the hydrogen–metal distance within the adsorbate–metal system, Yang and Whitten [30,31] concluded that the H—M interaction was in fact repulsive. They calculated vibrational frequencies and suggested that the 'soft' frequency occurred when the methyl group was tilted and moved away from the threefold centre to a position 0.07 eV higher in energy.

We believe that an important explanation lies in a model proposed by Gavin et al [40]. Using extended Huckel molecular orbital calculations, they found that upon adsorption, the most stable site for methyl will be that which achieves the maximum multicentre bonding. For CH_3, this is the hollow site, although similar calculations by other groups did not show a significantly strong interaction between the hydrogens and the surface atoms [41,42]. Here, we offer firm evidence for C—H—M multicentre bonding. On analysis of the methyl 1e derived quantum states in our calculations, it is clear that there is mixing between these and metal 3d states. The C—H bond can be viewed as an electron donor. The electrons in the C—H bond are attracted by the deep Ni 3d potential and delocalise into the region between the three atoms, holding them in a constrained environment with a lengthened C—H bond and a shortened H—Ni distance. It is possible that it is this lengthened C—H bond that is responsible for the 'soft' vibrational frequency. Fig. 9 shows an electron density contour plot and a three-dimensional isosurface of one of the 1e derived quantum states in CH_3/Ni(111). The energy of the 1e derived orbitals drop to an energy $\approx$6 eV below the Fermi level, being $\approx$2 eV lower than the corresponding

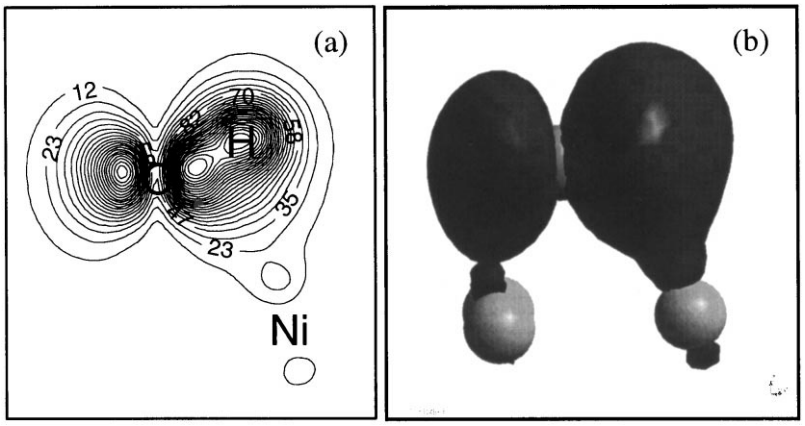

Fig. 9. Two-dimensional electron density contour plot (a) and a three-dimensional isosurface (b) highlighting C—H—Ni bonding. The 2D slice is perpendicular to the surface, cutting through the C—H—Ni three-centre bond. The density is plotted in units of 7.65×10^{-6} electrons bohr^{-3}.

orbitals in the gas phase. The charge delocalisation in these orbitals may be viewed as 'charge donation' from the C—H bonds of the methyl to the metal surface using classical chemistry terms.

On examination of multicentre bonding at the various sites, the strength of multicentre bonding appears to be dependent upon the hydrogen—nickel distance. The threefold hollow sites, which have the longest C—H bond lengths (1.10 Å), possess the strongest multicentre bonding and therefore the shortest H—Ni distance. The hcp60 and fcc60 sites, which have a shorter C—H bond length (1.09 Å), have a longer H—Ni distance. This relationship is clearly seen in the differing C—H bond lengths at the bridge site. The two C—H bonds closest to the bridging nickels are involved in strong three-centre bonding, whereas the third C—H bond, which is shorter, is involved in weaker three-centre bonding as it has a greater H—Ni distance (Fig. 3). Because of this interaction, the molecule is tilted. The molecule deforms and tilts so as to achieve maximum multicentre bonding for the two hydrogens (H_b and H_c) that are close to their nearest Ni neighbours at the expense of weaker multicentre bonding at the third H (H_a). At the top site where the H—Ni distance is large, the C—H bond is also found to have the shorter value of 1.09 Å. Therefore, it can be concluded that as the H—Ni distance decreases, multicentre bonding increases, and the C—H bond lengthens. This relationship is also seen in the structures obtained from the GGA and LDA structure optimisations, Table 4. The relationship is also borne out in the energy of the 1e–3d mixing states, being low when there is a short H—Ni distane and rising in energy as the H—Ni distance increases. The view of charge transfer from the C—H bond towards Ni is borne out in the charge densities around H. The density around H appears to be inversely proportional to the extent of three-centre bonding, tending to decrease as three-centre bonding increases.

The findings of Schule et al. [33] are also consistent with this view. They found a similar trend in C—H bond lengths: 1.10 and 1.09 Å for the fcc and top sites, respectively. They also found that the calculated C—H stretching frequency at the fcc site was $\approx 200\ \text{cm}^{-1}$ lower than at the top site. They suggested that this mode softening is a consequence of charge transfer from metal into C—H antibonding orbitals ($2e^*$). After a careful analysis of the quantum states in the system, however, we were unable to detect any significant occupation of C—H antibonding states. Schule et al. [33] also found that the C—H frequency is lower for fcc compared to fcc60. This is what we would expect as the H—Ni distance is shorter (and consequently the C—H bond in longer) in fcc than it is at fcc60.

The organometallic analogue of these solid-

state multicentre bonds may be the 'agostic' bond. Similar explanations have been offered for 'agostic' bonds [75]. In some alkyl complexes, the C—H bond has also been considered as an electron donor towards an electron deficient metal centre. In these 'agostic' bonding situations, longer C—H bond lengths and shorter M—H distances than the expected Van der Waals radii were also observed. In fact, a typical 'agostic' hydrogen can be part of a C—H bond that expands by up to 10%, and the M—H distances are typically in the region of 1.64–2.29 Å. The C—H bond lengths currently presented are not expanded as much as 'agostic' C—H bonds, which is reasonable since the H—M distances are somewhat longer. As we have seen upon rotation of CH_3 by 60°, at the threefold hollow sites, the energy increases by $\approx$0.2 eV (0.20 and 0.26 eV at the fcc and hcp sites, respectively). A quantum state analysis shows that the 1e derived states undergo the greatest energy increase upon rotation. The energies of the 2a1 derived states increase to a lesser extent, and the 3a1 derived states are essentially unaffected, i.e. a substantial proportion of the energy increase comes from a weakening of three-centre bonding. It appears, therefore, that three-centre bonding bond strengths are in this 0.2 eV region. In fact, upon rotation, the chemisorption energy at the hcp site is similar to that at the top site. Clearly, it is one of the reasons, possibly the main reason, why adsorption occurs at the hollow sites.

4. Conclusions

1. CH_3 binds strongly to all four high-symmetry adsorption sites of Ni(111) with calculated adsorption energies being 1.48, 1.46, 1.37, 1.24 eV for adsorption at the hcp, fcc, bridge and top sites, respectively. Consequently, the potential energy surface for CH_3 diffusion is fairly flat.
2. The preferred structure at the threefold sites is with the three hydrogens pointing towards their nearest Ni neighbours, and this arrangement is 0.20–0.26 eV more stable than when the hydrogens point towards their closest bridge sites. In the latter case, the hollow and top sites have similar stabilities.
3. Adsorbed CH_3 exhibits lengthened C—H bonds, and the exact length of these bonds depends on the adsorption site. These lengthened C—H bonds are one of the major reasons for the 'soft' C—H vibration. They occur because there is three-centre bonding between C—H—Ni. Three-centre bonding is a consequence of a charge delocalisation from C—H 1e orbitals towards Ni 3d states.
4. The extent of three-centre bonding is related to H—Ni distance, tending to increase as the H—Ni distance decreases. This results in strong three-centre bonding at the hollow sites and very weak three-centre bonding at the top site.
5. The main features in the bonding of CH_3 to the surface are:
   - Strong 3a1–3d mixing;
   - 1e–3d multicentre bonding;
   - weak 2a1–3d mixing
6. Due to the strong mixing of 3a1–3d and 1e–3d, there is a charge accumulation between C and Ni atoms, which is responsible for holding CH_3 on the surface. It appears that the major component of the chemisorption bond energy comes from 3a1–3d mixing and that 2a1 and 1e mixing helps to determine the preferred site for chemisorption.

Acknowledgements

The Supercomputing Centre for Ireland is gratefully acknowledged for computer time, and the authors wish to thank EPSRC for their financial support.

References

[1] W.A. Herrmann, Angew. Chem. Int. Ed. Engl. 21 (1982) 117.
[2] P. Biloen, W.M.H. Sachtler, Adv. Catal. 30 (1981) 165.
[3] W. Keim (Ed.), Catalysis in C_1 Chemistry, Reidel, Dordrecht, 1983.
[4] F. Fischer, H. Tropsch, Brennst. Chem. 7 (1926) 97.

[5] F. Fischer, H. Tropsch, Chem. Ber. 59 (1926) 830.
[6] A.E. Shilov, The Activation of Saturated Hydrocarbons by Transition Metal Complexes, Reidel, Dordrecht, 1984.
[7] R.G. Bergman, Science 28 (1984) 902.
[8] B.A. Arndsten, R.G. Bergman, T.A. Mobley, T.H. Peterson, Acc. Chem. Res. 28 (1995) 154.
[9] C.L. Hill (Ed.), Activation and Functionalisation of Alkanes, Wiley, New York, 1989.
[10] J.A. Davies, P.L. Watson, J.F. Liebman, A. Greenberg, Selective Hydrocarbon Activation, VCH, New York, 1990.
[11] A. Michaelides, P. Hu, A. Alavi, Physical origin for the high reactivity of subsurface hydrogen in catalytic hydrogenation, J. Chem. Phys., in press.
[12] F. Besenbacher, I. Chorkendorff, B.S. Clausen, B. Hammer, A.M. Molenbroek, J.K. Norskov, I. Stensgaard, Science 279 (1998) 1913.
[13] J.P. Van Hook, Catal. Rev. Sci. Eng. 21 (1980) 1.
[14] J.R. Anderson, M. Boudert (Eds.), Rostrup–Nielson, Catalysis — Science and Technology Vol. 5, Springer, Berlin, 1984, p. 1.
[15] M.P. Kaminsky, N. Winograd, G.L. Geoffroy, M.A. Vannice, J. Am. Chem. Soc. 108 (1986) 1315.
[16] M.B. Lee, Q.Y. Yang, S.T. Ceyer, J. Chem. Phys. 87 (1987) 2724.
[17] S.T. Ceyer, J.D. Beckerle, M.B. Lee, S.L. Tang, Q.Y. Yang, M.A. Hines, J. Vac. Sci. Technol. A 5 (1987) 501.
[18] Q.Y. Yang, S.T. Ceyer, J. Vac. Sci. Technol. A 6 (1988) 851.
[19] J.D. Beckerle, A.D. Johnson, Q.Y. Yang, S.T. Ceyer, J. Vac. Sci. Technol. A 6 (1988) 903.
[20] Q.Y. Yang, K.J. Maynard, A.D. Johnson, S.T. Ceyer, J. Chem. Phys. 102 (1995) 7734.
[21] F. Zaera, Chem. Rev. 95 (8) (1995) 2651.
[22] F. Zaera, Surf. Sci. 262 (1992) 335.
[23] F. Zaera, H. Hoffmann, J. Phys. Chem. 95 (1991) 6297.
[24] F. Zaera, Catal. Lett. 11 (1991) 95.
[25] F. Zaera, J. Vac. Sci. Technol. A 7 (1989) 640.
[26] C.-M. Chiang, T.H. Wentzlaff, B.E. Bent, J. Phys. Chem. 96 (1992) 1836.
[27] C.-M. Chiang, B.E. Bent, Surf. Sci. 279 (1992) 79.
[28] J.-L. Lin, B.E. Bent, J. Vac. Sci. Technol. A 10 (4) (1992) 2202.
[29] J.-L. Lin, B.E. Bent, Chem. Phys. Lett. 194 (1992) 208.
[30] H. Yang, J.L. Whitten, Surf. Sci. 255 (1991) 193.
[31] H. Yang, J.L. Whitten, J. Am. Chem. Soc. 113 (1991) 6442.
[32] P. Siegbahn, I. Panas, Surf. Sci. 240 (1990) 37.
[33] J. Schule, P. Siegbahn, U. Wahlgren, J. Chem. Phys. 8 (1988) 6982.
[34] H. Burghgraef, A.P.J. Jansen, R.A. van Santen, J. Chem. Phys. 98 (11) (1993) 8810.
[35] H. Burghgraef, A.P.J. Jansen, R.A. van Santen, Chem. Phys. 177 (1993) 407.
[36] H. Burghgraef, A.P.J. Jansen, R.A. van Santen, J. Chem. Phys. 101 (12) (1994) 11012.
[37] H. Burghgraef, A.P.J. Jansen, R.A. van Santen, Surf. Sci. 324 (1995) 345.
[38] A.D. Koster, R.A. van Santen, J. Catal. 127 (1991) 141.
[39] J.-F. Paul, P. Sautet, J. Phys. Chem. B 102 (1998) 1578.
[40] R.M. Gavin, J. Reutt, E.L. Muetterties, Proc. Natl. Acad. Sci. USA 78 (1981) 3981.
[41] C. Minot, M.A. van Hove, G.A. Somorjai, Surf. Sci. 127 (1982) 441.
[42] C. Zheng, Y. Apeloig, R. Hoffmann, J. Am. Chem. Soc. 110 (1988) 749.
[43] J.E. Demuth, H. Ibach, S. Lehwald, Phys. Rev. Lett. 40 (1978) 1044.
[44] M.A. Chesters, S.F. Parker, R. Raval, J. Electron Spectrosc. Relat. Phenom. 39 (1986) 155.
[45] R. Raval, M.A. Chesters, Surf. Sci. 219 (1989) L505.
[46] E. Cooper, A.M. Coats, R. Raval, J. Chem. Soc. Faraday Trans. 91 (20) (1995) 3703.
[47] F.M. Hoffmann, T.H. Upton, J. Phys. Chem. 88 (1984) 6209.
[48] M.C. Payne, M.P. Teter, D.C. Allen, T.A. Arias, J.D. Joannopolous, Rev. Mod. Phys. 64 (1992) 1045.
[49] M.J. Gillan, J. Phys. Condens. Matter 1 (1989) 689.
[50] A. de Vita, M.J. Gillan, J. Phys. Condens. Matter 3 (1991) 6225.
[51] D.M. Ceperly, B.J. Adler, Phys. Rev. Lett. 45 (1980) 566.
[52] J.P. Perdew, in: P. Ziesche, H. Eschrig (Eds.), Electronic Structure of Solids '91, Akademie Verlag, Berlin, 1991.
[53] J.P. Perdew, J.A. Chevary, S.H. Vosko, K.A. Jackson, D.J. Singh, C. Fiolhais, Phys. Rev. B 46 (1992) 6671.
[54] J.A. White, D.M. Bird, Phys. Rev. B 50 (1995) 4954.
[55] J. Goniakowski, J.M. Kantorovich, M.J. Gillan, J.A. White, Phys. Rev. B 53 (1996) 957.
[56] P.J.D. Lindan, N.M. Harrison, M.J. Gillan, W.A. White, Phys. Rev. B 55 (1997) 15919.
[57] S.P. Bates, M.J. Gillan, G. Kresse, J. Phys. Chem. B 102 (1998) 2017.
[58] A. Garcia, C. Elsasser, J. Zhu, S.G. Louie, M.L. Cohen, Phys. Rev. B 46 (1992) 9829.
[59] J.-S. Lin, A. Qteish, M.C. Payne, V. Heine, Phys. Rev. B 47 (1993) 4174.
[60] L. Kleinman, D.M. Bylander, Phys. Rev. Lett. 48 (1982) 1425.
[61] H.J. Monkhorst, J.D. Pack, Phys. Rev. B 13 (1976) 5188.
[62] D.R. Lide, Handbook of Chemistry and Physics, 78th edition, CRC Press, London, 1998.
[63] F. Passek, M. Donath, Phys. Rev. Lett. 71 (1993) 2122.
[64] M. Weinert, J.W. Davenport, Phys. Rev. Lett. 54 (1985) 1547.
[65] P. Kratzer, B. Hammer, J.K. Norskov, J. Chem. Phys. 105 (13) (1996) 5595.
[66] H.J. Zeiger, B. Wasserman, M.S. Dresselhaus, G. Dresselhaus, Surf. Sci. 124 (1983) 583.
[67] M.R. Shanabarger, Phys. Rev. Lett. 43 (1979) 1964.
[68] H.E. Dastoor, P. Gardner, D.A. King, Chem. Phys. Lett. 209 (1993) 493.
[69] H.P. Bonzel, G. Pirug, J.E. Muller, Phys. Rev. Lett. 58 (1987) 2138.
[70] J.E. Muller, Appl. Phys. A 49 (1989) 681.

[71] E. Schustorovich, R. Baetzold, E.L. Muetterties, J. Phys. Chem. 87 (1983) 1100.
[72] P. Hu, D.A. King, S. Crampin, M.H. Lee, M.C. Payne, Chem. Phys. Lett. 230 (1994) 501.
[73] P. Hu, D.A. King, M.H. Lee, M.C. Payne, Chem. Phys. Lett. 246 (1995) 73.
[74] P. Hu, D.A. King, S. Crampin, M.H. Lee, M.C. Payne, J. Chem. Phys. 107 (1997) 8103.
[75] M. Brookhart, M.L.H. Green, J. Organomet. Chem. 250 (1983) 395.
[76] R.D. Green, Hydrogen Bonding by C—H groups, Macmillan, New York, 1974.